Desalination and Water Treatment
www.deswater.com
doi: 10.5004/dwt.2020.25675

193 (2020) 83–94
July

Auto-combustion fabrication and characterization of TiO_2 nanoparticles and utilization as an adsorbent for removal of Pb^{2+} from aqueous solution

Ayman A. Ali, Esraa M. Elfiky*, Ibrahim S. Ahmed, Ahmed A. Khalil, Talaat Y. Mohamed

Chemistry Department, Faculty of Science, Benha University, Benha City, Egypt, Tel. +201064506103;
emails: esraao166@yahoo.com (E.M. Elfiky), ayman.abdelrazik@fsc.bu.edu.eg (A.A. Ali), isahmed2010@gmail.com (I.S. Ahmed), ahmed.khalil@fsc.bu.edu.eg (A.A. Khalil), talat.yehia@fsc.bu.edu.eg (T.Y. Mohamed)

Received 6 December 2019; Accepted 12 February 2020

ABSTRACT

Titanium oxide (TiO_2) was fabricated by using an auto-combustion technique with albumin egg fuel followed by calcination at 600°C for half an hour. TiO_2 nanoparticles were characterized by using various tools such as thermogravimetric analysis and differential thermal analysis, X-ray diffraction, energy dispersive X-ray analysis, scanning electron microscopy, transmission electron microscopy, and Fourier-transform infrared spectroscopy. The synthesized TiO_2 used as an adsorbent for Pb^{2+} removal from water. The removal of Pb^{2+} from water and adsorption capacity of the calcined TiO_2 nanoparticles was examined at different parameters. The model of adsorption isotherm and adsorption kinetics are used for the description of the removal of leads ions over the calcined TiO_2 nanoparticles.

Keywords: Nanoparticles; Auto-combustion technique; Adsorption; Morphology

1. Introduction

Environmental problems like water, air, and land contamination have spread due to rapid population growth and industrialization development. Heavy metals can be considered some of the most dangerous contaminants due to their non-biodegradable nature. Lately, water pollution by contaminated elements (e.g. Cr^{+2}, Hg^{+2}, Cd^{+2}, Zn^{+2}, As^{+2}, Cu^{+2}, Ni^{+2}, and Pb^{+2}) becomes one of the most extreme world problems [1–5]. These elements can describe as carcinogenic to individuals if these elements consumed in high dosage. Lead is a significant poisonous heavy metal that is utilized in galvanizing plants, metallurgy, varnishes and paints, battery and tannery manufacturing, pulp and paper industries, metal products, etc. Lead can be found as Pb^{2+} in H_2O that precipitates in soft tissues of the organism when extracting into food chains. Lead is a metabolic poison and enzyme inhibitor that precipitates in the brain, bones, kidney, and muscles. Hence it may cause big health issues like reduction in fertility, anemia, kidney failure, Alzheimer's disease, nervous system deterioration, and bone problems [6–8]. Nowadays, various methods are used for efficient pollutants and removal of contaminated metals from water by membrane and membrane ultrafiltration [9], coagulation–flocculation [10], reverse osmosis [11], precipitation and reduction [12], ion-exchange [13], electro-coagulation [14], electrodialysis [15] and adsorption [16]. If the concentrations of these metals are very high, these methods may be ineffective and also in general these methods are expensive [17]. The adsorption method is the most significant technique utilized for the treatment of water as it offers adaptability in operation and design, non-toxic, eco-friendly, inexpensive adsorbents, and also clean water treated with high quality in many cases [5,18,19].

Lately, many reports have appeared about simple and mixed metal oxides utilized as nano-adsorbents for removal of various poisonous metal particles (e.g. Hg^{2+}, and Pb^{2+})

* Corresponding author.

Presented at the 4th International Water Desalination Conference: Future of Water Desalination in Egypt and the Middle East, 24–27 February 2020, Cairo, Egypt

from water [20,21]. Nanosized metal oxides are the most widely studied as promising adsorbents (e.g. CeO_2, Fe_2O_3, MgO, Al_2O_3, MnO_2, ZnO, and TiO_2) which are classified as the important adsorbents for the removal of the contaminated metals from aqueous solutions. That is owing to their huge surface areas and large activities that can be a result of the size-quantization effect [22–25]. TiO_2 is considered a semiconducting material that generally utilized as an incredible adsorbent for the removal of a different elements like As(III) [26], Cu(II) [27], Cr(VI) [28], and Pb(II) [29]. Titania (TiO_2) nanoparticles get extensive consideration owing to its advantage of wide similarity, semiconducting properties [30] with large exciton binding energy, and unparalleled optical properties. These desirable properties make TiO_2 a possible candidate for many applications like Li-ion batteries, UV lasers, sensors, photodetectors, photocatalysts, and photovoltaic cells [31–34]. TiO_2 can be used as an exemplary semiconductor in photocatalysis because of its high oxidizing power and photostability [35].

Inorganic nanomaterials were produced by different methods such as sol–gel method [36], hydrothermal/solvothermal processes [37,38], vapor deposition [39], sonochemistry [40], microwave [41], combustion methods [42–44]. The fabricated materials were utilized in wide areas such as ecological research, energy research and biomedical engineering that is owing to their unparalleled characteristics like good mechanical properties, slow density, excellent resistance of corrosion, photochemical stability, very good biocompatibility, large strength-to-weight ratio and high catalytic efficiency [45]. In this study, titanium oxide (TiO_2) was fabricated by using an auto-combustion technique. TiO_2 nanoparticles were characterized by using various tools such as thermogravimetric analysis (TGA), differential thermal analysis (DTA), X-ray diffraction (XRD), energy dispersive X-ray analysis (EDX), scanning electron microscopy (SEM), transmission electron microscopy (TEM), and Fourier-transform infrared spectroscopy (FTIR). The synthesized TiO_2 was used as an adsorbent for (Pb^{2+}) removal from water. The synthesized TiO_2 used as an adsorbent for (Pb^{2+}) removal from water. And for (Pb^{2+}) removal from water adsorption capacity of the calcined TiO_2 nanoparticles was examined at numerous parameters. The various effects were examined by changing one variable while all other parameters remain fixed in the next sequence: pH on adsorption; contact time; dosage of adsorbent; metal concentration and temperature. The models of adsorption isotherm and adsorption kinetics are used for the description of the (Pb^{2+}) removal on the calcined TiO_2 nanoparticle surface.

2. Experimental

2.1. Materials and reagents

Lead nitrate ($Pb(NO_3)_2$, 99.95%), and titanium tetrachloride ($TiCl_4$, 99.9%) were produced from Sigma-Aldrich Company, Germany. Hydrochloric acid (HCl, 37%), ammonium hydroxide (NH_4OH, 33%), sodium hydroxide (NaOH, 98%) and albumin egg were also supplied from El. Nasr pharma chemicals Company, Cairo, Egypt. The reagents and chemicals which used in this research are analytical grade and all solutions were prepared by distilled water.

2.2. Fabrication of titanium oxide nanoparticles (TA)

Titanium oxide nanoparticles were fabricated utilizing the auto-combustion technique. Titanium hydroxide was obtained using the $TiCl_4$ solution (10 mL, 0.45 M) and dropwise from ammonium hydroxide with controlling pH of the solution at 9. The fabricated white precipitate was washed and separated following by adding the calculated moles of nitric acid (HNO_3) with stirring for 60 min till the white precipitate was completely dissolved. The obtained clear solutions were suspended with different weights of albumin egg (AE): (0.1, 0.25, 0.5, 0.75, and 1.0 g) with stirring for 10 min at 60°C. The synthesized suspensions were ignited at 250°C and the black, pale yellow and brown powder were obtained with the evolution of gases. The as-prepared powder was grinded and calcined at 600°C/30 min and the crystalline white titanium oxide nanoparticles were fabricated. Table 1 outlined the product names and compositions of the starting materials that utilized in the fabrication of the white TiO_2 nanoparticles. A flowchart of the fabricated TiO_2 nanoparticles appears in Fig. 1.

2.3. Batch adsorption studies

By using analytical-reagent grade, lead nitrate salt was used for the preparation of the stock solution of 1,000 mg/L of Pb^{2+} ions. This solution was diluted to suitable concentrations appropriately. All filtrated samples were analyzed using an atomic absorption spectrometer at a wavelength of 283.31 nm for (Pb^{2+}) ions. The effect of initial pH (1–8) on the lead ions adsorption was investigated using 0.050 g of TA adsorbent with 50 mL of 10 mg/L lead ions solution. The adsorbent with lead ions solution was stirred at 600 rpm for 24 h. After the separation using a centrifuge tool, the concentration of lead ions was determined after a particular experiment complete. The metal uptake and percentage removal were calculated using the next relationships:

$$Q_e = \left(C_0 - C_e\right)\frac{V}{m} \tag{1}$$

$$\%\ \text{adsorption} = 100\left\{\frac{C_0 - C_e}{C_e}\right\} \tag{2}$$

where C_0 and C_e are the initial and equilibrium concentrations of Pb(II) in mg/L. Q_e is the amount of Pb(II) adsorbed onto the unit mass of adsorbent in mg/g. V is the volume of the sample in L and m is the weight of (TA26 sample) in mg/L.

Table 1
Sample names and compositions of the starting materials which used in the synthesis of titanium oxide nanoparticles

Sample names	$TiCl_4$, g	AE, g	Ti^{4+}/AE, wt.%
TA1	0.855	0.1	1:8.55
TA2	0.855	0.25	1:3.42
TA3	0.855	0.5	1:1.71
TA4	0.855	0.75	1:1.14
TA5	0.855	1.00	1:0.855

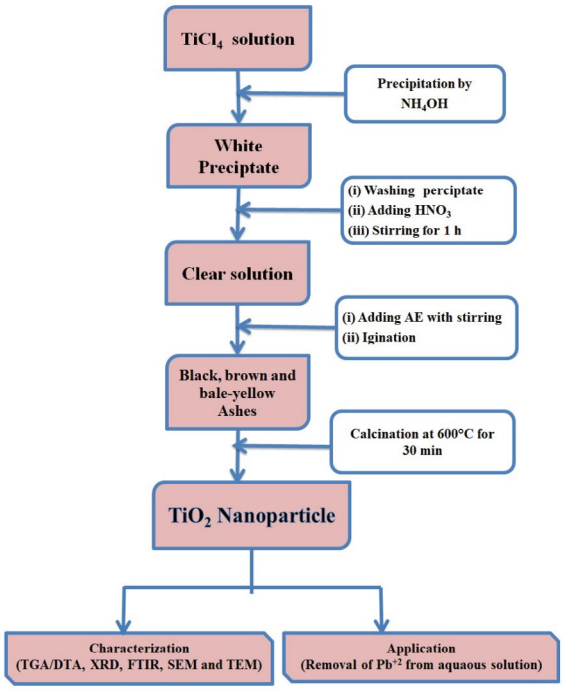

Fig. 1. Flowchart of the fabrication of titanium oxide nanoparticles by using combustion method.

2.4. Characterization

The as-fabricated and annealed sample was identified by using an XRD tool, 18 KW diffractometer (Bruker; model D8 advance) with monochromatic Cu-Ka radiation, 1.54178 (Å) in the angular range of 4°–80° with step size 0.02° (2θ) and scan step time 0.4 s. TG, DTA, and DTG are recorded to test the as-fabricated products and performed under air gas atmosphere using a thermal analyzer instrument (Shimadzu; model TA-60WS) with a heating rate of 10°C min^{-1} from room temperature to 700°C. The morphology of the calcined product was investigated utilizing field emission scanning electron microscope (FE-SEM, JEOL JSM–6390). The (FE-SEM) and gold coating process by using EMITECH K550X sputter coater. The morphology and particle size of the annealed samples were confirmed using high resolution (HR)-TEM (model Tecnai G20, FEI, Netherland) at an electron voltage of 200 kV. The as-fabricated and annealed products were measured using the FTIR spectrometer (Thermo Scientific; model Nicolet iS10) from 4,000 to 400 cm^{-1}. The adsorption processes were tested using an atomic absorption spectrometer (atomic absorption accessories, GTA120 Graphite Tube Atomizer, Agilent Company, USA) at a wavelength of 283.31 nm for (Pb^{2+}) ions.

3. Results and discussion

3.1. Characterization of the synthesized titanium oxide nano-adsorbent

3.1.1. TG-DTA analysis

Thermal analysis in the form of TGA, DTA, and DTG curves was investigated for an as-fabricated TA sample as seen in Fig. 2. DTG curve shows four peaks at 60°C, 205°C, 325°C, and 455°C according to the degradation of as-prepared materials. The decomposition of the TA sample (TG curve) happened in four steps as seen in Fig. 2. The total weight loss percentage was found to be 43.75% (36°C till 650°C). The first decomposition step happened in the range of 36°C–100°C which related to the removal of adsorbed volatile molecules (like H_2O) from the TA5 sample. The weight loss percentage found to be 6.25% in the first step. The second step appeared in the range of 100°C–250°C and the weight loss equals 15%. It explains that TA5 sample decomposed and the various gasses were evolved from the sample. 10% weight loss in the third stage and 12.5% in the fourth step in the TGA curve explained the removal of the back carbonaceous residual after the ignition of albumin. DTA curve of TA5 sample exhibited an endothermic peak at 65°C and four exothermic bands at 220°C, 350°C, 480°C, and 610°C. The DTA curve showed an endothermic peak at 65°C due to the separation of the volatile molecules from the surface of the TA5 sample. Besides, the exothermic peaks appeared in the range of 200°C–500°C with three heads at 220°C, 350°C, and 480°C. These peaks were attributed to the combustion of the residual of organic derivatives (albumin) with the evolution of the gases and the crystallization titanium oxide appeared from the as-fabricated amorphous titanium oxide of the TA5 sample. In addition, DTA showed the exothermic peak at 610°C due to the transformation of the anatase phase to the rutile phase of TiO_2 [46,47] and it agrees with XRD. From the extracted data from the thermal analysis, white titanium oxide nanoparticles were fabricated after the annealing at 600°C.

3.1.2. XRD studies

The XRD utilized for the examination of the crystal structure of the as-synthesized and calcined TiO_2 nanoparticle as be visible in Figs. 3a and b. The patterns appeared the effect of the calcination temperature on the phase and crystal size of synthesized TiO_2. The XRD patterns of the as-prepared TiO_2 nanoparticle have some diffraction peaks shown in Fig. 2a without any heat treatment. These diffraction peaks appeared at 25.28°, 37.80°, 46.05°, 53.9°, 55.03°, 62.67°, and 68.84° which related to 101, 004, 200, 105, 211, 204, and 116 for the diffraction planes of the anatase phase (TiO_2: tetragonal crystal structure; $a = b = 3.7822$, $c = 9.5023$ and $\alpha = \beta = \gamma = 90$) according to JCPDS or Reference card No. 84-1286. After calcination at 600°C and as shown in Fig. 3b, the anatase phase of TiO_2 according to JCPDS or Reference card No. 84-1286 was appeared and the other peaks with low intensity also were showed for the rutile phase of TiO_2 according to JCPDS or Reference cards No. 77-0446 and 87–07710 for TA16, TA26, and TA36 samples. The pure anatase phase structure of TiO_2 for TA46 and TA56 samples after the calcination at 600°C. The crystal sizes of TiO_2 determined by using the Debye–Scherrer formula as be visible in Eq. (3) [48]. The average crystallite size (D) of the as-prepared and calcined TiO_2 nanoparticles was recorded from the XRD peaks as outlined in Table 2.

$$D = \frac{0.9\lambda}{Z\cos\theta} \quad (3)$$

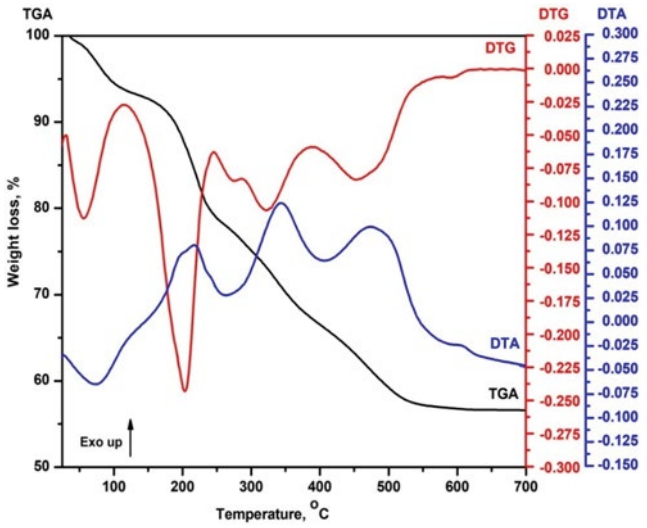

Fig. 2. Thermal analysis of the as-synthesized TA25 sample.

Table 2
Average crystallite size (S) of the as-prepared and calcined TiO_2 nanoparticles from the X-ray diffraction peaks

Samples no.	Average crystallite size, nm	
	As-prepared	After calcination
TA1	5.64	10.43
TA2	6.90	11.75
TA3	8.30	12.25
TA4	9.40	14.44
TA5	11.23	15.34

where, λ is the wavelength of X-ray (1.5406 A for Cu Kα), θ is the Bragg diffraction angle and Z is the X-ray full width of the diffraction peak at half-maximum height.

3.1.3. FTIR studies

Infrared spectra of the as-fabricated (TA1, TA2, TA3, TA4, and TA5 samples) and calcined TiO_2 nanoparticles (TA16, TA26, TA36, TA46, and TA56 samples) are shown in Figs. 3c and d. The peaks at 1,626–1,636 cm^{-1} and 3,400–3,500 cm^{-1} are related to the bending and the stretching vibrations of the adsorbed –OH groups, respectively as displayed in Fig. 3c. The peak at 1,100–1,120 cm^{-1}, 1,350–1,400 $cm^{-1,}$ and 2,853–2,925 cm^{-1} can be characterized for the symmetric vibration of C–O–C, C=O, and aliphatic CH. In the spectra of the as-prepared samples and without heat treatment, the peaks in between 400–900 cm^{-1} (at 553–566–580–606–644 cm^{-1} for all samples) correspond to the vibration modes of Ti–O inside TiO_2 lattice. In Fig. 3d shows the spectra of the calcined sample: TA16, TA26, TA36, TA46, and TA56. The weak absorption bands at 3,424–3,380 cm^{-1} and 1,626–1,635 cm^{-1} are corresponding to the stretching and bending vibrations of OH groups, respectively. The weak bands at 1,100–1,135 cm^{-1} appeared in the spectra for and assigned to the symmetric vibration of carbon–oxygen–carbon. In the spectra of the calcined samples, the bands at 450–470 cm^{-1}, 580–680 cm^{-1}, and 800–820 cm^{-1} appeared for all samples which are related to the vibration modes of Ti–O inside TiO_2 lattice [46,47].

3.1.4. Morphology of the calcined titanium oxide nanoparticles

The HR-TEM and FE-SEM images of the calcined TiO_2 nanoparticle (TA26 sample) are displayed in Figs. 4a–d. The micrographs of SEM showed that the morphology of the calcined titanium oxide nanoparticles has a large and porous spherical shape with agglomeration. The small particle sizes are determined from micrographs and found to be 17 nm [49]. The small spherical nanoparticles are agglomerated with each other and the large size one was built in the size of 1 μm. Images of TEM appeared the various morphology shape of the synthesized TA26 sample. TEM images of TiO_2 nanoparticles showed the spherical and square shape as shown in Figs. 4e–h. It can be estimated that the particle size of the TA26 sample found to be 14 nm. The extracted data from the TEM agree with XRD analysis (cal. 12 nm) and it showed that the TA26 sample has soft agglomeration.

EDX graph and the elemental analysis of TA26 displayed in Fig. 4i. EDX graph showed the two lines corresponding to two elements: Ti and O. The elemental composition of TA26 with 48.50% for the Ti element and 51.50% for O element. The percentage of Ti and O elements suggested the presence of these elements in the form of the TiO_2 compound. From the spectrum, it is evident that no other peak corresponding to impurities was detected, which indicates the high purity of the synthesized titanium oxide nanoparticles.

3.2. Adsorption studies

3.2.1. Adsorption parameters studies

The effect of the pH (1.0–8.0) on the adsorption of Pb ions (50 ml of 20 mg/L) over 50 mg of the synthesized TA26 was investigated at room temperature as displayed in Fig. 5a. The adsorption of Pb ions from solution on TA26 adsorbent and the removal percentage increased from 10% to 97.75% when the pH value of the solution was raised from 1 to 5 after 24 h. The removal efficiency values remain almost constant as the pH value increased. The adsorption behavior might be explained in this point by the protonation and deprotonation of active sites on the surface of the TA26 sample. At lower pH, the surface TA26 sample was highly protonated which decreased the metal adsorption. Whereas at higher pH the (TA) surface becomes negatively charged due to deprotonation caused by the presence of OH groups in the solution. At higher pH, the electrostatic interaction between negatively charged of the TA26 surface and positively charged lead ions increased which promoted adsorption. Moreover, the precipitation of Pb ions from the solution as lead hydroxide at a pH greater than 6.0 and could have resulted in increased adsorption.

Therefore, for the elimination of precipitation effect and for considering the only adsorption efficiency, the pH of lead ions solutions was kept lower than the critical pH of hydroxide precipitation. Therefore, the optimum pH

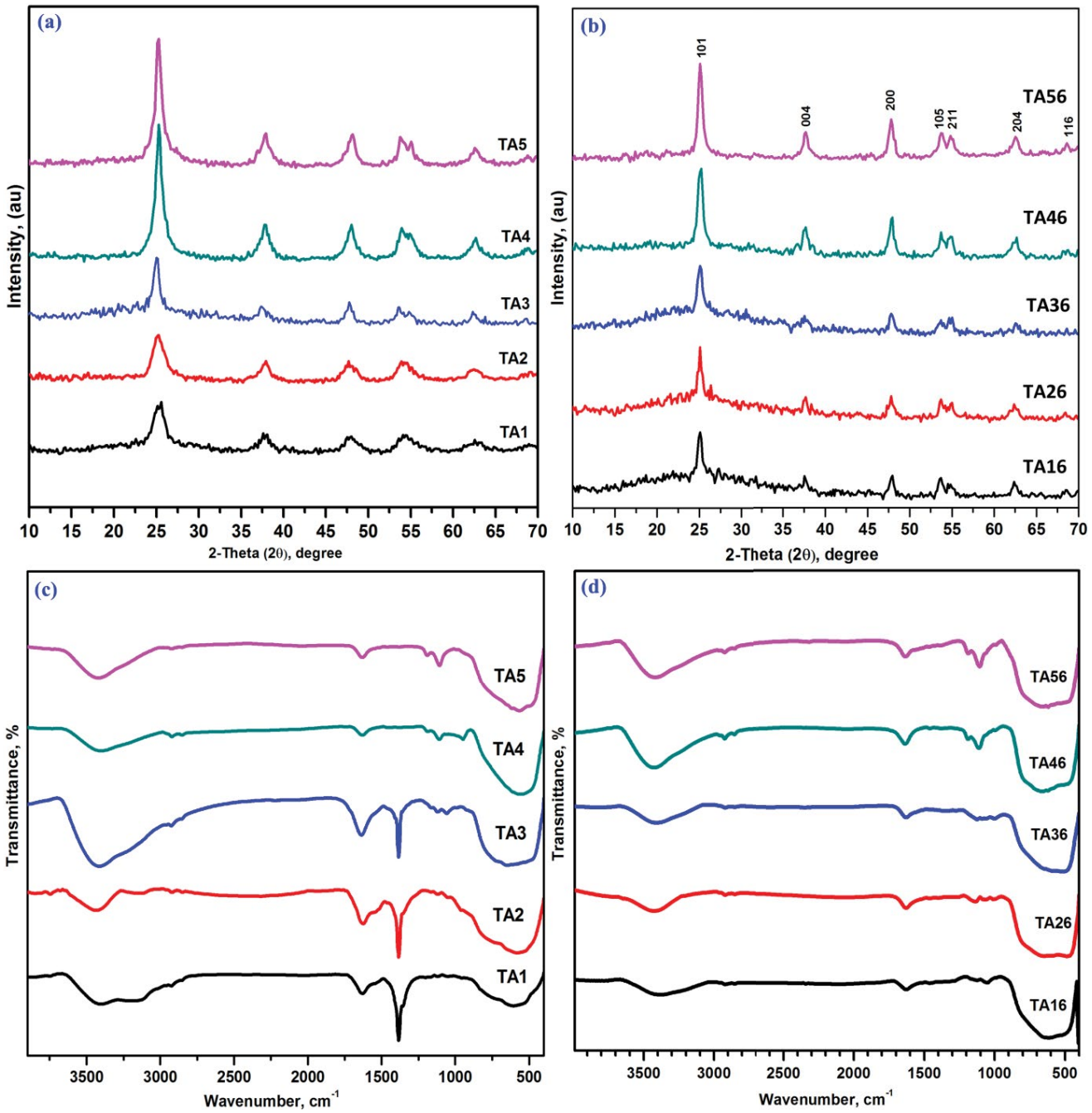

Fig. 3. XRD analysis (a and b) and FTIR analysis (c and d) of the synthesized titanium oxide samples.

was chosen at 4.5 for the removal of lead ions from aqueous solution [50]. Fig. 5 shows the effect of the time on the adsorption capacity of the removal of Pb ions in the concentrations range: (10–150 mg/L) over 50 mg of TA26 with contact time range 10–300 min at pH 4.5 and room temperature. As shown in Fig. 5b, the adsorption capacity of the removal of lead ions using TA26 samples increased while the contact time was raised from 10 to 60 min. With raising the contact time up to 60 min., the adsorption capacity increased slowly till it becomes constant at 120 min for all concentrations. The first step of the removal was fast over the surface synthesized TiO_2 nanoparticles for the free of active sides, while the active pores on the surface of adsorbent were filled in the second step and the rate became slower and almost reached to the saturation [51]. Fig. 5c shows the effect of the dosage of TA26 sample: 0.025–0.125 g/L was carried out for the removal of 60 mg/L of Pb ions after 120 min at room temperature and pH 4.5. As shown in Fig. 5c, the removal of Pb ions was decreased from 31.9 to 18.1 mg/g as a result of the weight of the TA26 sample increased from 25 to 125 mg. Therefore, 50 mg is considered the perfect adsorbent dose for the removal of Pb ions from aqueous solution [8]. Fig. 5d

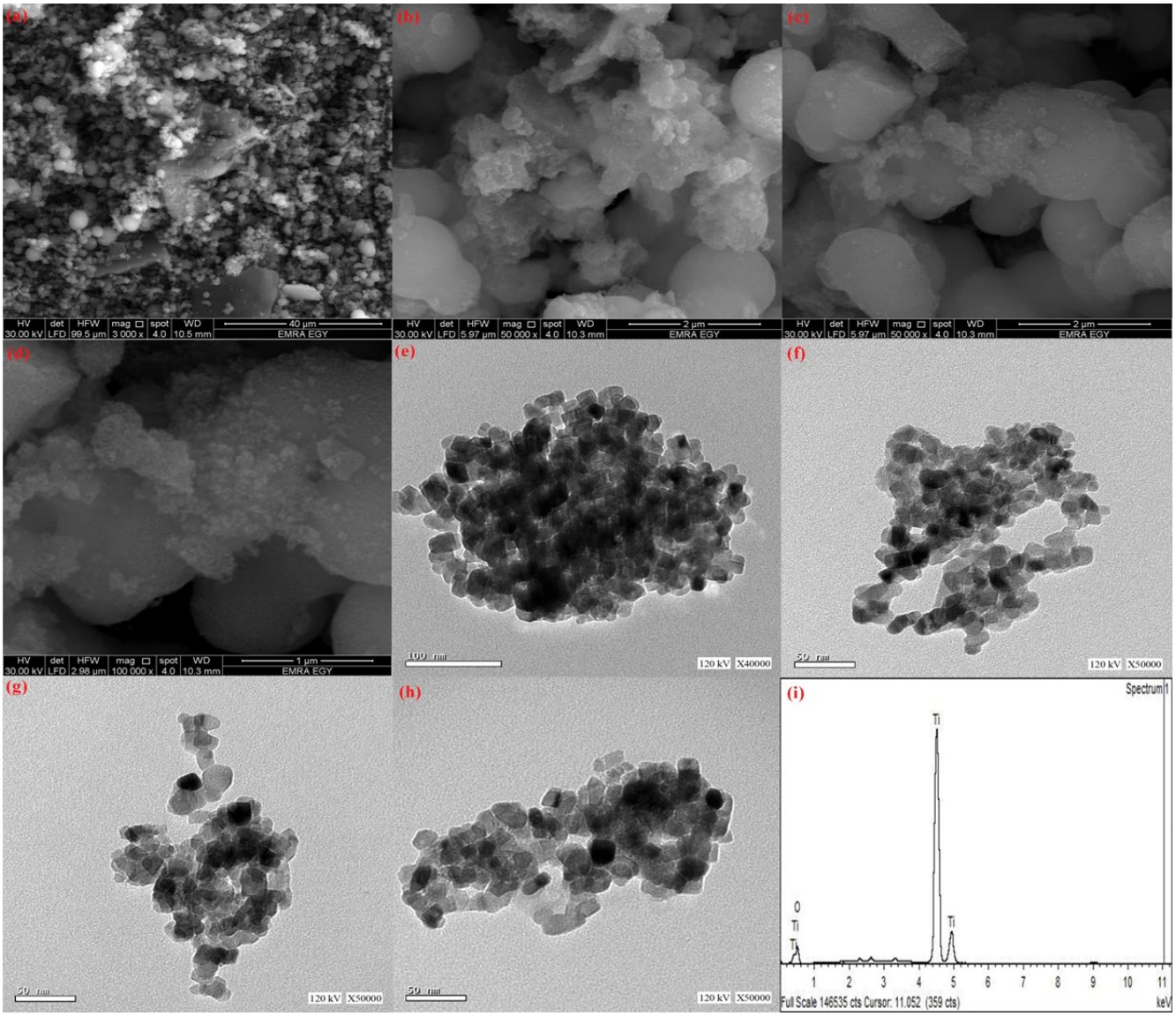

Fig. 4. (a–d) FE-SEM images, (e–h) HR-TEM images, and (i) EDX graph of the calcined titanium oxide (TA26 sample).

shows the temperature factor (25°C, 40°C, and 50°C) on the adsorption of lead ions (60 mg/L) over 50 mg of TA26 after 90 min at pH 4.5. As shown in Fig. 5d, the adsorption decreases almost for the removal of lead ions when the temperature was raised from 25°C to 50°C, indicating the exothermic nature of the adsorption process. This could be due to activation and faster movement of Pb^{2+} ions toward the coordinating sites of TA26 adsorbent at low temperature.

3.3. Isotherm studies

Langmuir, Freundlich and Temkin isotherm models were utilized for the explanation of the removal of the Pb^{2+} ion over the synthesized TA26 sample from an aqueous solution according to Eqs. (4)–(6).

$$\frac{C_e}{q_e} = \frac{1}{K_L q_m} + \frac{C_e}{q_m} \tag{4}$$

$$\ln\left(q_e\right) = \ln K_F + \frac{1}{B}\ln C_e \tag{5}$$

$$q_e = Z\ln K_T + Z\ln C_e \tag{6}$$

where C_e is the equilibrium concentration of lead ions in the solution, q_e (mg/g) is the amount of Pb^{2+} ion adsorbed per unit weight of the adsorbent, K_b (L/mg) is the Langmuir constant, q_m ($q_m = K_F C_0^{1/B}$ mg/g) is the maximum capacity of led ions adsorbed per unit weight of adsorbent [52], C_0 is initial concentration, K_F is Freundlich constants (mg/g), $1/B$ is heterogeneity factor, B represents adsorption intensity which varies with a heterogeneity of the adsorbent surface and for a favorable adsorption process B should be in the range of 1–10 [53], R is the universal gas constant (8.341 J/mol/K), T is the temperature in Kelvin, K_T (L/g) and Z ($Z = RT/b$ kJ/mol) are Temkin constants and b is the heat of adsorption.

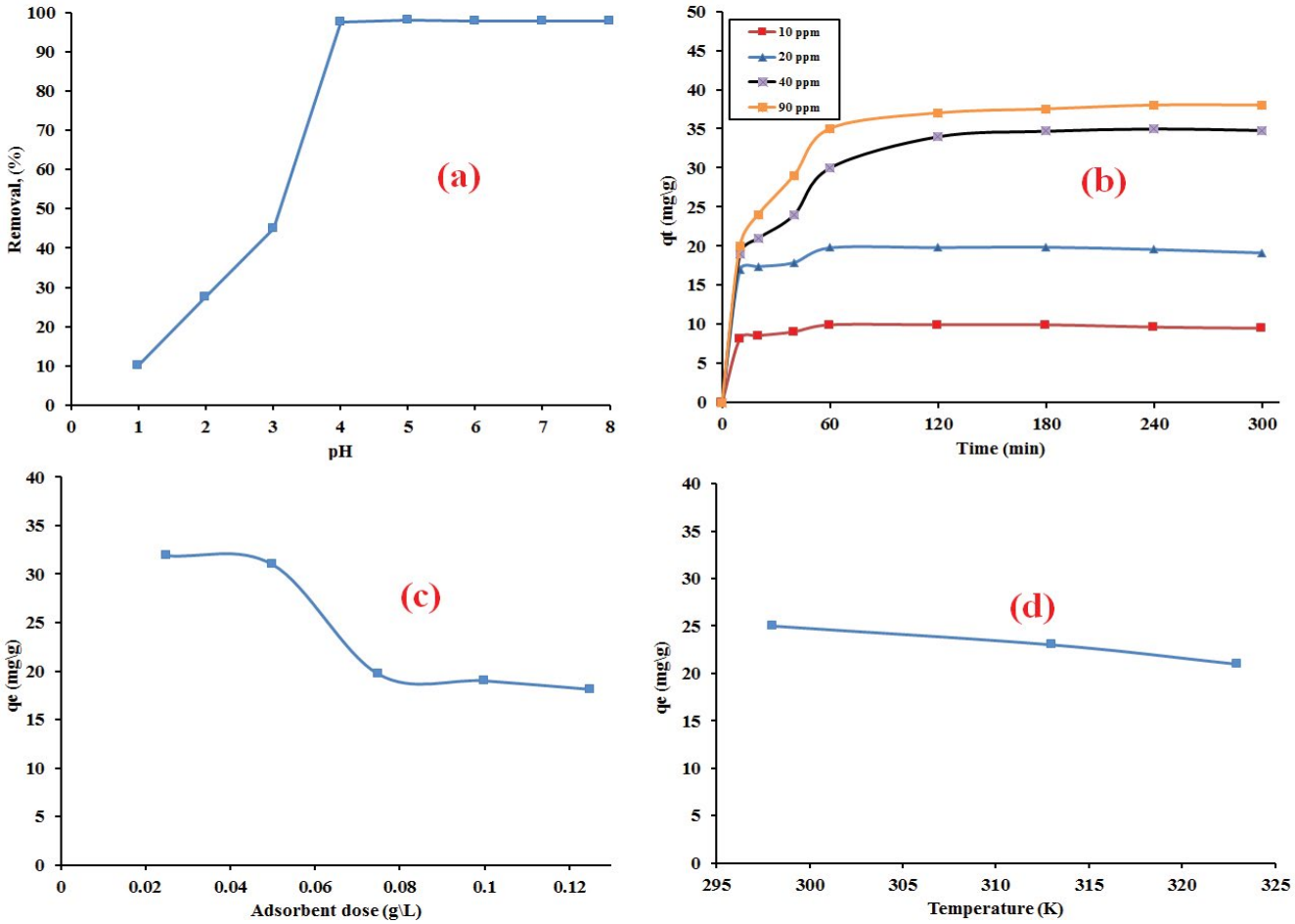

Fig. 5. (a) Effect of pH, (b) time with different initial concentration, (c) adsorbent dose, and (d) temperature on the removal of the lead ions over the titanium oxide nanoparticle.

Figs. 6b–d shows the isotherm models: from Langmuir (C_e/q_e with C_e), Freundlich ($\ln q_e$ with $\ln C_e$), and Temkin (q_e with $\ln C_e$) for the separation of lead ions from aqueous solution or the synthesized TA26 sample. Table 3 outlines the extracted parameters from the isotherm models. R_L values determined from Langmuir constant K_L and initial concentration of lead ions and their values reflected the favorable adsorption process (R_L = 0–1) [18]. From the R^2 values of the tested isotherms, Langmuir isotherm model is better fitting than the other isotherms. It explains that the adsorption of the lead ions over the TiO_2 nano-adsorbent was formed the monolayer without any interaction between adsorbed molecules. Also, the extracted adsorption capacity using Langmuir isotherm was calculated to be 38 mg/g which is close to the experimental value (38.16 mg/g). Herein, R_L values were determined between 0.00299–0.0431, related to the initial concentration of 10–150 mg/L. It explains that the removal of the lead ions over the TA26 sample is a favorable adsorption process.

3.4. Adsorption kinetic studies

Kinetic study of the adsorption process of lead ions from aqueous solution to give information about the rate of the reaction and the adsorption mechanism. The mechanism of the adsorption process depends on the physical and chemical characteristics of the adsorbent and adsorbate. The mechanism and rate of adsorption were proposed by fitting the experimental kinetic data to pseudo-first-order ($\log(q_e–q_t)$ and t), pseudo-second-order (t/q_t and time t) [54] and intraparticle diffusion model (q_t and $t^{0.5}$) [55] as represented in Eqs. (7)–(9).

$$\log\left(q_e - q_t\right) = \log q_e - \frac{K_F}{2.303}t \tag{7}$$

$$\frac{t}{q_t} = \frac{1}{K_S q_e^2} + \frac{t}{q_e} \tag{8}$$

$$q_t = K_{ID}t^{0.5} + E \tag{9}$$

where q_e and q_t are the weight of lead ions adsorbed (mg/g) at equilibrium and contact time t (min), respectively, K_F is the pseudo-first-order rate constant of adsorption (min^{-1}), K_S (g/mg min) is pseudo-second-order rate adsorption constant, K_{ID} is intraparticle diffusion constant (mg/g $min^{0.5}$),

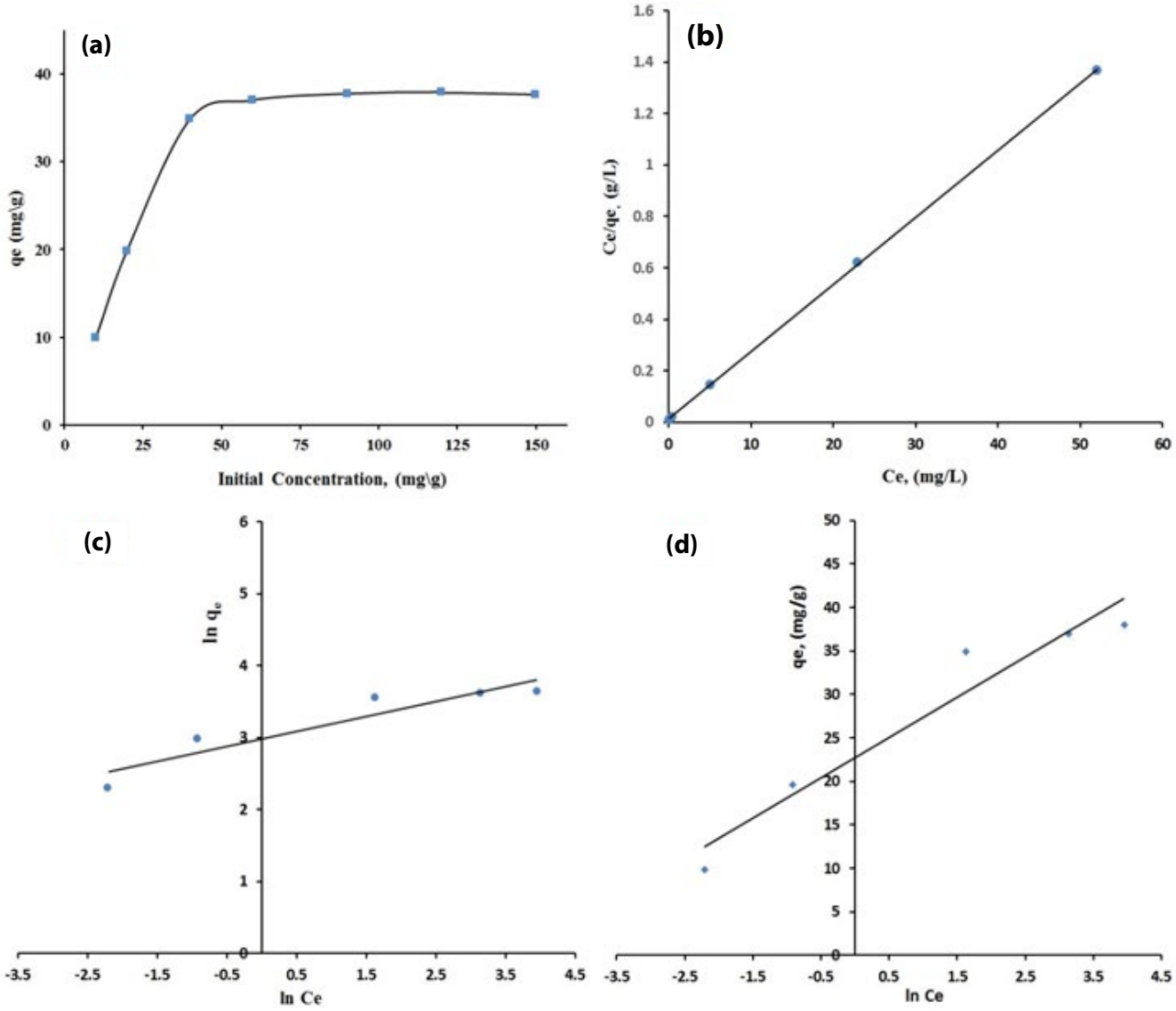

Fig. 6. (a) Effect of initial concentration on the adsorption capacity, (b) Langmuir, (c) Freundlich, and (d) Temkin isotherms for removal of the lead ions over TA26 sample.

and E is constant that gives an idea about the thickness of boundary layer (mg/g).

Figs. 7a–c display the kinetic relations of the separated lead ions and the extracted kinetic factors are outlined in Table 4. According to the values of R^2 for the tested experimental data using various models, the pseudo-second-order model is the better fitting (R^2 = 0.999) than the pseudo-first-order (R^2 = 0.956) for the removal of the lead ions over TiO_2 nano-adsorbent [54]. So, we can say that the extraction of lead ions from aqueous solution TiO_2 follows the pseudo-second-order model, and the adsorption capacity value: 39.62 mg/g is in good agreement with the calculated from the experimental data: 38 mg/g. Fig. 7c exhibits the intraparticle diffusion model and the values from the relation: K_{ID} = 3.2 mg/g min$^{0.5}$ and E = 9.66 mg/g. The linear relation does not pass the origin point and it is explained that the intraparticle diffusion cannot use for the illustration mechanism of the removal of lead ions from the solution over TA26 nano-adsorbent.

3.5. Adsorption thermodynamics

Thermodynamic parameters including Gibbs free energy change ($\Delta G°$), enthalpy change ($\Delta H°$) and entropy change ($\Delta S°$) were calculated to evaluate the feasibility and nature of the adsorption process. Thermodynamics parameters of the adsorption of lead ions from their solutions over the TA26 sample were tested using van't Hoff equation (Eq. (12); lnK_c and 1/T) [56] at 25°C, 40°C, and 50°C as shown in Fig. 7d.

$$\Delta G° = -RT \ln K_c \tag{10}$$

$$\Delta G° = \Delta H° - T\Delta S° \tag{11}$$

Table 3
Extracted parameters from the tested isotherms for TiO_2 nano-adsorbent (TA26 sample)

Adsorption isotherm	Parameter	Value of parameter
Langmuir parameters	K_L (L/mg)	2.22
	$q_{m\ (cal)}$ (mg/g)	38.16
	R_L	0.00299–0.0431
	R^2	0.9999
	$q_{m\ (exp)}$ (mg/g)	38
Freundlich parameters	K_F [(L/mg) (L/mg)$^{1/B}$]	19.71
	$q_{m\ (cal)}$ (mg/g)	50.21
	B	4.81
	R^2	0.8755
	$q_{m\ (exp)}$ (mg/g)	38
Temkin parameters	K_T (L/g)	136.4
	b (KJ/mol)	0.5362
	Z (J/mol)	4.62
	R^2	0.9383

$$\ln K_c = \frac{\Delta S^\circ}{R} - \frac{\Delta H^\circ}{RT} \tag{12}$$

where the values of K_c were extracted from q_e/C_e and are the equilibrium constant (L/g), T is the temperature in Kelvin (k) and R is the gas constant (8.314 J/mol). The extracted of lead ions using TA26 adsorbent was exothermic process according to the negative charge of ΔH°. The value of ΔH° (cal. 9.014 KJ/mol) is lower than 40 KJ/mol, the removal of lead ions over the TA26 sample is the physisorption adsorption process. ΔS° has a negative charge (0.033 KJ/mol) which means the decrease in the degree of freedom of solution for the separation process. The positive values of ΔG° reflected that the adsorption process of lead ions is a non-spontaneous process. Besides, the ΔG° values increased with rising of the temperature and it means that the extraction of lead ions is unfavorable at high temperatures.

3.6. Comparison with other adsorbents

The adsorption capacity of adsorbent under study is compared to that of other adsorbents reported in the literature [50,57–62] and the extracted data are outlined

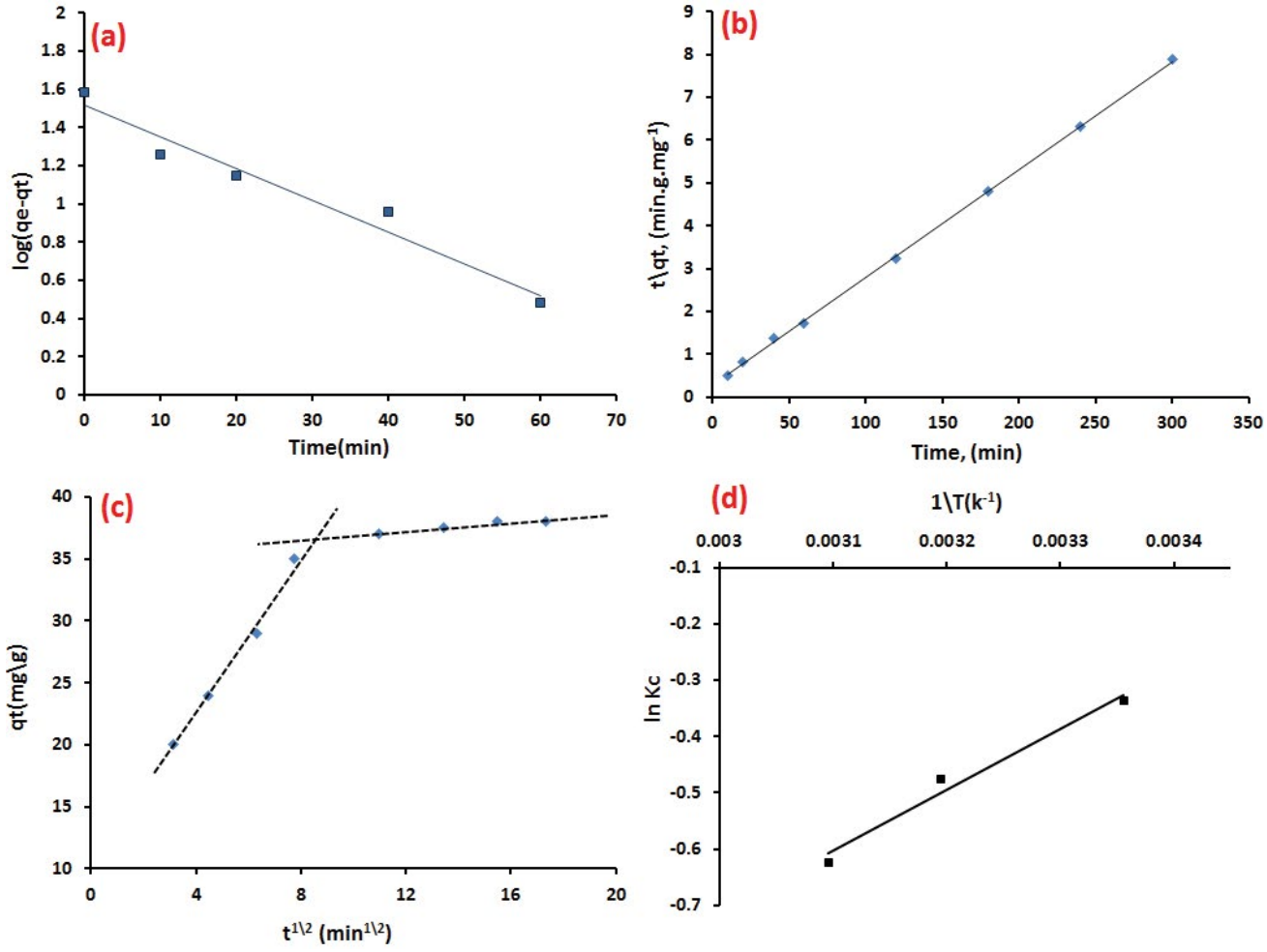

Fig. 7. (a) Pseudo-first-order model, (b) pseudo-second-order model, (c) intra-particle diffusion model, and (d) lnK_c against 1/T for adsorption of lead ions using TA26 sample.

Table 4
Kinetic parameters for adsorption of Pb^{2+} over the synthesized TA26 adsorbent

Kinetic model	Parameter	Extracted parameters
Pseudo-first-order	K_S (min^{-1})	0.0235
	$q_{m\ (cal)}$ (mg/g)	22.719
	R^2	0.956
	$q_{m\ (exp)}$ (mg/g)	38
Pseudo-second-order	K_S (g/mg.min)	0.000637
	$q_{m\ (cal)}$ (mg/g)	39.618
	R^2	0.999
	$q_{m\ (exp)}$ (mg/g)	38
Intra-particle diffusion	K_{IF} (mg/g $min^{0.5}$)	3.2
	E (mg/g)	9.66
	R^2	0.9908

Table 5
Thermodynamic parameters for the adsorption of Pb(II) on the synthesized adsorbent

Temperature, (°K)	$\ln K_c$	$\Delta G°$	$\Delta H°$	$\Delta S°$
		(KJ/mol)	(KJ/mol)	(KJ/mol)
298	–0.33647	0.8094		
313	–0.47542	1.3039	–9.0137	–0.03296
323	–0.62417	1.6335		

Table 6
Comparison between the synthesized TiO_2 (TA) oxide nano-adsorbent and other adsorbents

Adsorbent	q_m (mg/g)	Reference
Fe_2O_3/Al_2O_3	23.75	[50]
Chitosan-GLA beads	14.24	[57]
Chitosan beads	34.98	[57]
(Graphene) GNS	22.42	[58]
GNS500	35.21	[58]
GNS700	35.46	[58]
ZnO	26.109	[59]
Hydrous amorphous/γ-Fe_2O_3	19.2	[60]
Fe_3O_4	29.0	[61]
CeO_2	9.2	[62]
TiO_2 (TA56)	38	Present work

in Table 5. The capacity value of the tested TA26 sample from the experimental data in our study is higher than other adsorbents (Table 6).

4. Conclusions

Titanium oxide (TiO_2) nanoparticles were synthesized by using auto-combustion technique and albumin egg fuel following by calcination at 600°C. The synthesized TiO_2 nanoparticles were characterized by various tools such as TGA, DTA, XRD, EDX, SEM, TEM, and FTIR. The synthesized TiO_2 used as an adsorbent for the removal (Pb^{2+}) from aqueous media. Langmuir isotherm model is better fitting than the other isotherms and the adsorption capacity of the calcined TiO_2 nanoparticles was found to be 38 mg/g. The pseudo-second-order model is the better fitting (R^2 = 0.999) than the pseudo-first-order (R^2 = 0.956) for the removal of the lead ions over TiO_2 nano-adsorbent. The removal of lead ions using TA26 adsorbent was an exothermic process according to the negative charge of $\Delta H°$ and it is the physisorption process. The adsorption process of lead ions is a nonspontaneous process and it is unfavorable adsorption process at high temperatures.

References

[1] L. Villegas, Removal of Heavy Metals from Aqueous Solution by Biofilm-Forming Bacteria Isolated from Mined-Out Soil in Mogpog, Marinduque, Philippines, 2018.
[2] M. Karnib, A. Kabbani, H. Holail, Z. Olama, Heavy metals removal using activated carbon, silica and silica activated carbon composite, Energy Procedia, 50 (2014) 113–120.
[3] G. Gyananath, D. Balhal, Removal of lead(II) from aqueous solutions by adsorption onto chitosan beads, Cellul. Chem. Technol., 46 (2012) 121.
[4] F.N. Azad, M. Ghaedi, K. Dashtian, S. Hajati, A. Goudarzi, M. Jamshidi, Enhanced simultaneous removal of malachite green and safranin O by ZnO nanorod-loaded activated carbon: modeling, optimization, and adsorption isotherms, New J. Chem., 39 (2015) 7998–8005.
[5] N. Ilankoon, Use of iron oxide magnetic nanosorbents for Cr(VI) removal from aqueous solutions: a review, J. Eng. Res. Appl., 4 (2014) 55–63.
[6] A. Asfaram, M. Ghaedi, A. Goudarzi, M. Rajabi, Response surface methodology approach for optimization of simultaneous dye and metal ion ultrasound-assisted adsorption onto Mn-doped Fe_3O_4-NPs loaded on AC: kinetic and isothermal studies, Dalton Trans., 44 (2015) 14707–14723.
[7] A. Navas-Acien, E. Guallar, E.K. Silbergeld, S.J. Rothenberg, Lead exposure, and cardiovascular disease—a systematic review, Environ. Health Perspect., 115 (2006) 472–482.
[8] S.A. Chaudhry, T.A. Khan, I. Ali, Adsorptive removal of Pb(II), and Zn(II) from water onto manganese oxide-coated sand: isotherm, thermodynamic and kinetic studies, Egypt. J. Basic Appl. Sci., 3 (2016) 287–300.
[9] S. Malamis, E. Katsou, M. Stylianou, K. Haralambous, M. Loizidou, Copper removal from sludge permeate with ultra-filtration membranes using zeolite, bentonite, and vermiculite as adsorbents, Water Sci. Technol., 61 (2010) 581–589.
[10] F.M. Pang, P. Kumar, T.T. Teng, A.M. Omar, K.L. Wasewar, Removal of lead, zinc, and iron by coagulation–flocculation, J. Taiwan Inst. Chem. Eng., 42 (2011) 809–815.
[11] Y. Benito, M. Ruiz, Reverse osmosis applied to metal finishing wastewater, Desalination, 142 (2002) 229–234.
[12] E. Katsou, S. Malamis, K.J. Haralambous, Industrial wastewater pre-treatment for heavy metal reduction by employing a sorbent-assisted ultrafiltration system, Chemosphere, 82 (2011) 557–564.
[13] A. Dąbrowski, Z. Hubicki, P. Podkościelny, E. Robens, Selective removal of the heavy metal ions from waters and industrial wastewaters by ion-exchange method, Chemosphere, 56 (2004) 91–106.
[14] N. Adhoum, L. Monser, N. Bellakhal, J.-E. Belgaied, Treatment of electroplating wastewater containing Cu^{2+}, Zn^{2+}, and Cr(VI) by electrocoagulation, J. Hazard. Mater., 112 (2004) 207–213.
[15] T. Mohammadi, A. Razmi, M. Sadrzadeh, Effect of operating parameters on Pb^{2+} separation from wastewater using electrodialysis, Desalination, 167 (2004) 379–385.

[16] İ. Şahin, S.Y. Keskin, C.S. Keskin, Biosorption of cadmium, manganese, nickel, lead, and zinc ions by *Aspergillus tamarii*, Desal. Water Treat., 51 (2013) 4524–4529.
[17] T.A. Khan, S.A. Chaudhry, I. Ali, Equilibrium uptake, isotherm and kinetic studies of Cd(II) adsorption onto iron oxide activated red mud from aqueous solution, J. Mol. Liq., 202 (2015) 165–175.
[18] T.A. Khan, S.A. Chaudhry, I. Ali, Thermodynamic and kinetic studies of As(V) removal from water by zirconium oxide-coated marine sand, Environ. Sci. Pollut. Res., 20 (2013) 5425–5440.
[19] S. Dashamiri, M. Ghaedi, K. Dashtian, M.R. Rahimi, A. Goudarzi, R. Jannesar, Ultrasonic enhancement of the simultaneous removal of quaternary toxic organic dyes by CuO nanoparticles loaded on activated carbon: central composite design, kinetic and isotherm study, Ultrason. Sonochem., 31 (2016) 546–557.
[20] O. Hakami, Y. Zhang, C.J. Banks, Thiol-functionalised mesoporous silica-coated magnetite nanoparticles for high-efficiency removal and recovery of Hg from water, Water Res., 46 (2012) 3913–3922.
[21] S. Singh, K. Barick, D. Bahadur, Surface engineered magnetic nanoparticles for removal of toxic metal ions and bacterial pathogens, J. Hazard. Mater., 192 (2011) 1539–1547.
[22] M. Hua, S. Zhang, B. Pan, W. Zhang, L. Lv, Q. Zhang, Heavy metal removal from water/wastewater by nanosized metal oxides: a review, J. Hazard. Mater., 211 (2012) 317–331.
[23] X. Qu, P.J. Alvarez, Q. Li, Applications of nanotechnology in water and wastewater treatment, Water Res., 47 (2013) 3931–3946.
[24] R. Taman, M. Ossman, M. Mansour, H. Farag, Metal oxide nanoparticles as an adsorbent for removal of heavy metals, J. Adv. Chem. Eng., 5 (2015) 1–8.
[25] X. Wang, Y. Guo, L. Yang, M. Han, J. Zhao, X. Cheng, Nanomaterials as sorbents to remove heavy metal ions in wastewater treatment, J. Environ. Anal. Toxicol., 2 (2012) 1000154.
[26] C. Jing, X. Meng, E. Calvache, G. Jiang, Remediation of organic and inorganic arsenic-contaminated groundwater using a nanocrystalline TiO_2-based adsorbent, Environ. Pollut., 157 (2009) 2514–2519.
[27] M. Visa, A. Duta, TiO_2/fly ash novel substrate for simultaneous removal of heavy metals and surfactants, Chem. Eng. J., 223 (2013) 860–868.
[28] K. Parida, K.G. Mishra, S.K. Dash, Adsorption of toxic metal ion Cr(VI) from aqueous state by TiO_2-MCM-41: equilibrium and kinetic studies, J. Hazard. Mater., 241 (2012) 395–403.
[29] K.E. Engates, H.J. Shipley, Adsorption of Pb, Cd, Cu, Zn, and Ni to titanium dioxide nanoparticles: effect of particle size, solid concentration, and exhaustion, Environ. Sci. Pollut. Res., 18 (2011) 386–395.
[30] J.-M. Herrmann, Photocatalysis fundamentals revisited to avoid several misconceptions, Appl. Catal., B, 99 (2010) 461–468.
[31] W. Zhou, L. Gai, P. Hu, J. Cui, X. Liu, D. Wang, G. Li, H. Jiang, D. Liu, H. Liu, Phase transformation of TiO_2 nanobelts and TiO_2(B)/anatase interface heterostructure nanobelts with enhanced photocatalytic activity, Cryst. Eng. Comm., 13 (2011) 6643–6649.
[32] M. Müllner, J. Yuan, S. Weiss, A. Walther, M. Förtsch, M. Drechsler, A.H. Müller, Water-soluble organo−silica hybrid nanotubes templated by cylindrical polymer brushes, J. Am. Chem. Soc., 132 (2010) 16587–16592.
[33] Y. Wu, J. Yu, H.-M. Liu, B.-Q. Xu, One-dimensional TiO_2 nanomaterials: preparation and catalytic applications, J. Nanosci. Nanotechnol., 10 (2010) 6707–6719.
[34] M. Yu, Y.-Z. Long, B. Sun, Z. Fan, Recent advances in solar cells based on one-dimensional nanostructure arrays, Nanoscale, 4 (2012) 2783–2796.
[35] S.M. Gupta, M. Tripathi, A review of TiO_2 nanoparticles, Chin. Sci. Bull., 56 (2011) 1639.
[36] V. Loryuenyong, K. Angamnuaysiri, J. Sukcharoenpong, A. Suwannasri, Sol–gel derived mesoporous titania nanoparticles: effects of calcination temperature and alcoholic solvent on the photocatalytic behavior, Ceram. Int., 38 (2012) 2233–2237.
[37] X. Feng, J. Zhai, L. Jiang, The fabrication and switchable superhydrophobicity of TiO_2 nanorod films, Angew. Chem. Int. Ed., 44 (2005) 5115–5118.
[38] M. Wei, Y. Konishi, H. Zhou, H. Sugihara, H. Arakawa, A simple method to synthesize nanowires titanium dioxide from layered titanate particles, Chem. Phys. Lett., 400 (2004) 231–234.
[39] S. Mathur, V. Sivakov, H. Shen, S. Barth, C. Cavelius, A. Nilsson, P. Kuhn, Nanostructured films of iron, tin and titanium oxides by chemical vapor deposition, Thin Solid Films, 502 (2006) 88–93.
[40] J. Guo, S. Zhu, Z. Chen, Y. Li, Z. Yu, Q. Liu, J. Li, C. Feng, D. Zhang, Sonochemical synthesis of TiO_2 nanoparticles on graphene for use as photocatalyst, Ultrason. Sonochem., 18 (2011) 1082–1090.
[41] Y. Zheng, K. Lv, Z. Wang, K. Deng, M. Li, Microwave-assisted rapid synthesis of anatase TiO_2 nanocrystals with exposed {0 0 1} facets, J. Mol. Catal. A: Chem., 356 (2012) 137–143.
[42] A.A. Ali, I.S. Ahmed, Sol–gel auto-combustion fabrication and optical properties of cobalt orthosilicate: utilization as coloring agent in polymer and ceramic, Mater. Chem. Phys., 238 (2019) 121888.
[43] A. Ali, E. El Fadaly, I.S. Ahmed, Near-infrared reflecting blue inorganic nano-pigment based on cobalt aluminate spinel via combustion synthesis method, Dyes Pigm., 158 (2018) 451–462.
[44] A. Ali, B. Karasu, M. Allazov, T. Ilyasli, Synthesis, characterization, and study of the effect of Yb^{3+} on $MgAl_2O_4$ spinel structure via combustion method, J. Chem., 3 (2013) 133–138.
[45] S. Wu, Z. Weng, X. Liu, K. Yeung, P.K. Chu, Functionalized TiO_2 based nanomaterials for biomedical applications, Adv. Funct. Mater., 24 (2014) 5464–5481.
[46] F. Jahantigh, M. Nazirzadeh, Synthesis and characterization of TiO_2 nanoparticles with polycarbonate and investigation of its mechanical properties, Int. J. Nanosci., 16 (2017) 1750012.
[47] M. Viana, V. Soares, N. Mohallem, Synthesis and characterization of TiO_2 nanoparticles, Ceram. Int., 36 (2010) 2047–2053.
[48] P. Scherrer, Göttinger Nachrichten Math, Physics, 2 (1918) 98–100.
[49] G. Li, L. Lv, H. Fan, J. Ma, Y. Li, Y. Wan, X. Zhao, Effect of the agglomeration of TiO_2 nanoparticles on their photocatalytic performance in the aqueous phase, J. Colloid Interface Sci., 348 (2010) 342–347.
[50] K. Zargoosh, H. Abedini, A. Abdolmaleki, M.R. Molavian, Effective removal of heavy metal ions from industrial wastes using thiosalicylhydrazide-modified magnetic nanoparticles, Ind. Eng. Chem. Res., 52 (2013) 14944–14954.
[51] R. Balasubramanian, S. Perumal, K. Vijayaraghavan, Equilibrium isotherm studies for the multicomponent adsorption of lead, zinc, and cadmium onto Indonesian peat, Ind. Eng. Chem. Res., 48 (2009) 2093–2099.
[52] F.N. Azad, M. Ghaedi, K. Dashtian, S. Hajati, V. Pezeshkpour, Ultrasonically assisted hydrothermal synthesis of activated carbon–HKUST-1-MOF hybrid for efficient simultaneous ultrasound-assisted removal of ternary organic dyes and antibacterial investigation: Taguchi optimization, Ultrason. Sonochem., 31 (2016) 383–393.
[53] M. Ghaedi, H.Z. Khafri, A. Asfaram, A. Goudarzi, Response surface methodology approach for optimization of adsorption of Janus green B from aqueous solution onto ZnO/Zn$(OH)_2$-NP-AC: kinetic and isotherm study, Spectrochim. Acta, Part A, 152 (2016) 233–240.
[54] M. Ghaedi, H. Mazaheri, S. Khodadoust, S. Hajati, M. Purkait, Application of central composite design for simultaneous removal of Methylene blue and Pb^{2+} ions by walnut wood activated carbon, Spectrochim. Acta, Part A, 135 (2015) 479–490.
[55] Y. Zhu, J. Hu, J. Wang, Competitive adsorption of Pb(II), Cu(II), and Zn(II) onto xanthate-modified magnetic chitosan, J. Hazard. Mater., 221 (2012) 155–161.
[56] J.V. Milojković, M.L. Mihajlović, M.D. Stojanović, Z.R. Lopičić, M.S. Petrović, T.D. Šoštarić, M.Đ. Ristić, Pb(II) removal from aqueous solution by *Myriophyllum spicatum* and its compost: equilibrium, kinetic and thermodynamic study, J. Chem. Technol. Biotechnol., 89 (2014) 662–670.

[57] W.W. Ngah, S. Fatinathan, Pb(II) biosorption using chitosan and chitosan derivatives beads: equilibrium, ion exchange, and mechanism studies, J. Environ. Sci., 22 (2010) 338–346.
[58] Z.-H. Huang, X. Zheng, W. Lv, M. Wang, Q.-H. Yang, F. Kang, Adsorption of lead(II) ions from aqueous solution on low-temperature exfoliated graphene nanosheets, Langmuir, 27 (2011) 7558–7562.
[59] V. Venkatesham, G. Madhu, S. Satyanarayana, H. Preetham, Adsorption of lead on gel combustion derived nano ZnO, Procedia Eng., 51 (2013) 308–313.
[60] M. Fan, T. Boonfueng, Y. Xu, L. Axe, T.A. Tyson, Modeling Pb sorption to microporous amorphous oxides as discrete particles and coatings, J. Colloid Interface Sci., 281 (2005) 39–48.
[61] N.N. Nassar, Rapid removal and recovery of Pb(II) from wastewater by magnetic nanoadsorbents, J. Hazard. Mater., 184 (2010) 538–546.
[62] H. Cao, J. Chen, J. Zhang, H. Zhang, L. Qiao, Y. Men, Heavy metals in rice and garden vegetables and their potential health risks to inhabitants in the vicinity of an industrial zone in Jiangsu, China, J. Environ. Sci., 22 (2010) 1792–1799.